Biogeosciences Discuss., 10, 13977–14007, 2013
www.biogeosciences-discuss.net/10/13977/2013/
doi:10.5194/bgd-10-13977-2013

Biogeosciences Discussions
Open Access

Synthesis of observed air–sea CO_2 exchange fluxes in the river-dominated East China Sea and improved estimates of annual and seasonal net mean fluxes

C.-M. Tseng[1], P.-Y. Shen[1], and K.-K. Liu[2]

[1]Institute of Oceanography, National Taiwan University, Taipei 106, Taiwan
[2]Institute of Hydrological & Oceanic Sciences, National Central University, Jungli, Taoyuan 320, Taiwan

Received: 3 July 2013 – Accepted: 12 August 2013 – Published: 26 August 2013

Correspondence to: C.-M. Tseng (cmtseng99@ntu.edu.tw)

Published by Copernicus Publications on behalf of the European Geosciences Union.

Abstract

Limited observations exist for reliable assessment of annual CO_2 uptake that takes into consideration the strong seasonal variation in the river-dominated East China Sea (ECS). Here we explore seasonally representative CO_2 uptakes by the whole East China Sea derived from observations over a 14 yr period. We firstly identified the biological sequestration of CO_2 taking place in the highly productive, nutrient-enriched Changjiang river plume, dictated by the Changjiang river discharge in warm seasons. We have therefore established an empirical algorithm as a function of sea surface temperature (SST) and Changjiang river discharge (CRD) for predicting sea surface pCO_2. Synthesis based on both observation and model show that the annually averaged CO_2 uptake from atmosphere during 1998–2011 was constrained to about 1.9 mol C m^{-2} yr^{-1}. This assessment of annual CO_2 uptake is more reliable and representative, compared to previous estimates, in terms of temporal and spatial coverage. Additionally, the CO_2 time-series, exhibiting distinct seasonal pattern, gives mean fluxes of −3.0, −1.0, −0.9 and −2.5 mol C m^{-2} yr^{-1} in spring, summer, fall and winter, respectively, and also reveals apparent inter-annual variations. The flux seasonality shows a strong sink in spring and a weak source in late summer-early fall. The weak sink status during warm periods in summer-fall is fairly sensitive to changes of pCO_2 and may easily shift from a sink to a source altered by environmental changes under climate change and anthropogenic forcing.

1 Introduction

Continental shelves generally receive large loads of carbon from land on the one hand and sustain rapid biological growth and biogeochemical cycling with rates much higher than those in the open ocean, on the other hand (Walsh, 1991). Despite their relatively small total surface area (~ 8 % of the whole ocean area), they overall play a significant role in the global biogeochemical cycle as a net sink of atmospheric

BGD
10, 13977–14007, 2013

CO_2 ($0.2 \sim 0.5\,GtC\,yr^{-1}$), which represents $10 \sim 30\,\%$ of the current estimate of global oceanic CO_2 uptake (Borges et al., 2005; Cai et al., 2006; Chen and Borges, 2009; Laruelle et al., 2010). In addition, the coastal seawaters interact and exchange strongly in complex ways with the atmosphere, and the open ocean. Thus, the environment complexities and diversity of the shelf seas pose a challenge to characterization of the dynamic carbon cycling in these regions. Based on literature compilations and global extrapolation in estimates of CO_2 sequestration in marginal seas, the aforementioned estimates existed with large uncertainties. That is because many regions are grossly under-sampled, especially the mid-latitude continental shelves (Borge et al., 2010).

It was reported continental shelves at mid- and high-latitudes generally act as a sink for atmospheric CO_2, while as a source of CO_2 at low latitudes, between 30° S–30° N. The East China Sea (ECS) is situated between the low- and mid-latitudes (between 25° N–34° N) with estimated overall CO_2 sink strength of $1 \sim 3\,mol\,C\,m^{-2}\,yr^{-1}$ (Peng, et al., 1999; Tsunogai et al., 1999; Wang et al., 2000; Shim et al., 2007; Zhai and Dai, 2009; Tseng et al., 2011). As a whole, the ECS ($\sim 0.2\,\%$ of global ocean area) could yield annual carbon uptake of $0.01 \sim 0.03\,GtC$, representing $0.5 \sim 2.0\,\%$ of the global uptake. This implies a relatively high CO_2 uptake rate compared to other ocean regions. Previously reported air–sea CO_2 fluxes were, however, biased by inadequate spatial and/or temporal coverage. For instance, Tsunogai et al. (1999) first showed estimates of $\sim 3\,mol\,C\,m^{-2}\,yr^{-1}$ uptake of the ECS from atmospheric CO_2 based on extrapolating from a single transect data of the PN line across the central ECS. Other later CO_2 flux studies in the ECS with uptake rates of $1 \sim 3\,mol\,C\,m^{-2}\,yr^{-1}$ had been spatially limited as well (Fig. 1a). Moreover, a reliable quantification in seasonally representative CO_2 uptakes by the whole ECS has not been established to date.

The observational requirements to adequately investigate air–sea CO_2 exchange for the ECS are challenging due to the high spatial and temporal heterogeneity and complexity of the physical and biogeochemical processes (Liu et al., 2003, 2010). Sea surface pCO_2 (pCO_{2w}) distribution in the ECS are spatially/temporally variable as a result of interactions among the seasonal thermal cycle, net community produc-

BGD
10, 13977–14007, 2013

tion/respiration, surface/subsurface sea waters and river waters. The dominant processes in the ECS vary by seasons and regions, with typically active biological uptake of CO_2 in warm periods and intensely physical mixing and solubility of CO_2 in the cold seasons (Tseng et al., 2011; Chou et al., 2011). In addition, pCO_{2w} distribution is subjected to mixing of varied water masses which are characterized by the nutrient-rich and less saline Changjiang Diluted water (CDW, waters within 31 – isohaline) and warm, saline and nutrient-depleted Kuroshio (KW), shelf mixed (SMW) and Taiwan Warm Current (TWC) waters (Fig. 1b). Consequently, the mixing of water masses with different biogeochemical characteristics in the ECS causes the spatial/temporal CO_2 variations (e.g., Tseng et al., 2011). Further, various circulation regimes lead to the shelf-edge processes for material exchange between the East China Sea Shelf and the adjoining Kuroshio (e.g., Liu et al., 2010). Thus, to enable better quantification of the ECS CO_2 uptake capacity reiterates the need of greater spatial and temporal resolutions in observational data, which are needed for accurate estimation of air–sea CO_2 fluxes in the ECS over an annual cycle.

This study presents new data and expands on the approach of Tseng et al. (2011) of adopting innovative methods to extend the spatial and temporal coverage for broad scale assessments of distribution and air–sea exchange fluxes of CO_2. A regional synthesis based on satellite remote sensing data (e.g., sea surface temperature, SST) calibrated with direct near surface underway pCO_2 measurements and modified by the Changjiang (a.k. a Yangtze) river discharge (CRD) has therefore been established. The CRD as the dominant freshening nutrient source of the ECS played a key influence on modulating the CO_2 uptake (Tseng et al., 2011). We found firstly an empirical relationship for predicting water pCO_2 as a function of CRD and SST. The relation was then applied to the whole ECS shelf (25–33.5° N and 122–129° E) after the model generated pCO_{2w} results had been well validated against the observed pCO_{2w}. The resultant algorithm aimed to improve the quantification of shelf CO_2 uptake capacity in the ECS eventually leads to a time-series of the air–sea CO_2 exchange flux from 1998

BGD
10, 13977–14007, 2013

to 2011 that yield an annual mean value of unsurpassed accuracy after an examination of different gas-transfer algorithms.

2 Materials and methods

2.1 Analytical methods and data analyses

Twelve seasonal cruises for direct underway atmospheric (pCO_{2a}) and water pCO_2 (pCO_{2w}) with hydrographic measurements were carried out in the East China Sea (ECS) shelf (25–32° N and 120–128° E) between June 2003 and July 2011 on board R/V *Ocean Researcher I*. There was also one earlier cruise in July 1998 performing similar measurements. Most cruises (n = 9) were conducted in warm seasons that allowed delineation of the effects of discharge variations on the CO_2 uptake, whereas there were also cruises conducted in each of the other seasons (spring, fall and winter). Additional data were obtained to provide the complete seasonal coverage of CO_2 distribution in the ECS.

The cruise tracks and hydrographic stations superimposed on main surface currents in this study area are shown in Fig. 1b. The underway system with continuous flow equilibration, provided by the National Oceanic and Atmospheric Administration (NOAA) of the United States, is fully automated and uses gas standards (the xCO_2 of the four standards was 266.56, 301.76, 406.72, and 451.37 ppm, respectively) from NOAA (Wanninkhof, 1993). Precision and accuracy achieved with this method are ±0.1 and ±2 µatm, respectively. The distributions of sea surface salinity (SSS) and temperature (SST) were recorded using a SBE21 SEACAT thermosalinograph system (Sea-Bird Electronics Inc.). Surface chlorophyll *a* (chl *a*) concentration was measured with a Sea Tech fluorometer attached to the SeaBird CTD for a continuous in-vivo fluorescence, with data calibrated by in-vitro fluorometry (Turner Design 10-AU-005). Nutrient (e.g., nitrate+nitrite) and chl *a* concentrations were measured according to Gong et al. (1996) and Tseng et al. (2005).

BGD
10, 13977–14007, 2013

The time-series records including remotely sensed SST data, archived hydrographic salinity (Japan Oceanographic Data Center, JODC), wind speed (at PenGaYi Islet; 25.62° N, 122.07° E), Changjiang river discharge (CRD, Datong hydrological gauge station; 30.76° N, 117.62° E) and air pCO_2 data (JeJu Island, South Korea; 33.28° N, 126.15° E) for estimating pCO_{2w} with related air–sea exchange flux in the ECS region (25–33.5° N and 122–129° E) were briefly described as below. The weekly average SST data were derived from the Advanced Very-High Resolution Radiometer (AVHRR) images from the NOAA with 1 km × 1 km resolution (http://www.osdpd.noaa.gov/ml/ocean/sst.html). The AVHRR-SST agreed well with ship-board observations (Tseng et al., 2007, 2009a, b). The archived hydrographic salinity data in the ECS were provided by Japan Oceanographic Data Center (JODC) with data resolution of 1° × 1° grids (http://jdoss1.jodc.go.jp/cgi-bin/1997/bss). The monthly wind speed data were estimated from the daily average data at land-based weather station of PenGaYi Islet (25.62° N, 122.07° E) in the ECS provided by the Taiwan Central Weather Bureau (TCWB). The monthly CRD data at Datong hydrological gauge station (30.76° N, 117.62° E) in the lower reach of Changjing were obtained from the Hydrological information Centre of China. The air pCO_2 was estimated from the monthly atmospheric xCO_2 (mole fraction) measured at JeJu Island (South Korea; 33.28° N, 126.15° E), after correction for water vapor pressure at 100 % humidity with SST and salinity data (http://www.esrl.noaa.gov/gmd/ccgg/globalview/).

2.2 Air-sea CO_2 exchange flux estimates

Air–sea exchange flux, F, of pCO_2 is estimated using the equation: $F = K \times \delta pCO_2$, where K (gas transfer coefficient) = kL (k: transfer velocity; L: gas solubility), δpCO_2 is the difference between the pCO_2 of surface water and air (i.e., $pCO_{2w} - pCO_{2a}$). The pCO_{2a} was estimated from the monthly average pCO_2 observed at JeJu Island during the study period. Solubility of CO_2 as a function of water temperature and salinity can be estimated from the Weiss (1974) empirical equation. To obtain a more representative flux, gas transfer velocity (k) is derived using the Wanninkhof (1992) empirical

BGD
10, 13977–14007, 2013

relationship: $k = 0.31 \times u^2 \times (Sc/660)^{-0.5}$, where Schmit number ($Sc$) is temperature-dependant for CO_2 in seawater, computed from in situ temperature data and u is the wind speed at 10 m height obtained from PenGaYi station (monthly average wind data from the TCWB database of 1998–2011). The parameterization of Wanninkhof (1992), representing a reasonable estimate for calculating wind-induced k, was firstly used for comparison with previous flux estimates in the ECS. Then, the air–sea exchange fluxes of CO_2 in the ECS reported in the previous studies were re-calculated according to the consistent wind speed data and Wanninkhof's algorithm used in this study. Finally, uncertainties of CO_2 fluxes due to using different gas-transfer algorithms (e.g., Liss and Merlivat, 1986; Wanninkhof, 1992; Wanninkhof and McGillis, 1999; Jacobs et al., 1999; Nightingale et al., 2000; McGillis et al., 2004; Ho et al., 2006; Wanninkhof et al., 2009) and their appropriate flux ranges in the ECS shelf were quantitatively evaluated.

2.3 Areal mean of pCO_2 and environmental variables

To obtain a representative mean value for the ECS shelf, we prepared the interpolated data set of $0.01^\circ \times 0.01^\circ$ (about 1 km × 1 km) grid points from observed pCO_2 and other environmental variables (e.g., SST, Salinity, N+N, chl *a* etc.) by kriging and then calculated the areal means by integrating over the survey area. The grid resolution matches the spatial resolution of weekly AVHRR-SST data. For the areal mean of the air–sea flux, we first calculated the flux within a given grid box along the cruise track for underway pCO_2 measurement using the average values of SST, salinity, and δpCO_2 in the box and the monthly average wind speed; then, we calculated the areal mean CO_2 flux over the study area in the same fashion mentioned above. Likewise, we computed the flux estimates for the model study regions, encompassing almost the entire ECS (i.e., Region B: 25–33.5° N and 122–129° E, Fig. 1a).

BGD
10, 13977–14007, 2013

3 Results and discussion

3.1 Representativeness of the study region

The East China Sea (ECS) is a large marginal sea (25–33.5° N, 120–129.5° E) in the northwestern Pacific with an area of $\sim 0.6 \times 10^6$ km^2, of which 3/4 is a wide continental shelf (Fig. 1a). Our cruise region is situated in the southern and western ECS, covering an area about a half of the whole ECS. In order to evaluate whether the cruise data are representative of the entire ECS, we compared the areal mean values of AVHRR-SST from the two model areas against the observed average SST data. The two areas are respectively a small one (Region S, 25–31.5° N and 123–126° E), which is similar to the cruise survey area and a bigger one (Region B, 25–33.5° N and 122–129° E), which covers almost the whole ECS (Fig. 1a). Briefly, the areal mean SST calculated from observed values in cruise survey area correlated well with the average AVHRR-SST data in two model domains with perfect regression relationships ($R^2 = 0.96$) as shown respectively in Fig. 2a and b. It indicates, on the one hand, the remotely sensed SST data used here are reliable and validated in terms of data assurance; on the other hand, the areal mean SST data obtained on our cruise investigations can represent the variability of the areal mean value of the entire ECS. Therefore, it is reasonable to assume that the relationship between the areal means of pCO_2 and mean values of hydrographic variables obtained on our cruises was also representative for the entire ECS. Further, we may use the aforementioned relationship to derive representative average values of pCO_2 for Region B, which should be the most representative for the ECS shelf.

3.2 Summer CO_2 uptake determined by Changjiang river discharge

Figure 1c and d shows the composite distributions of pCO_{2w} and air–sea CO_2 exchange flux from nine cruises in summer between 2003 and 2011. As reported previously and shown in Fig. 1, the pCO_{2w} distribution in the ECS was associated with

BGD
10, 13977–14007, 2013

variations of water masses (Tseng et al., 2011). Lower pCO_{2w} values were observed in the CDW plume area near the Changjiang river mouth and higher values in the south-eastern shelf area, where saline and nutrient-depleted Kuroshio, Shelf Mixed Water and Taiwan Warm Current Water prevailed. Also, the distribution of CO_2 flux in the ECS resembled that of pCO_2. More negative values (i.e., uptake of atmospheric CO_2 by surface water) were mostly found in the nutrient-rich river plume area with a gradual increase to the east and south. Despite the high sea surface temperature in summer that favored release of CO_2 to the atmosphere, the Changjiang river plume acted as a strong CO_2 sink, mainly due to CO_2 drawdown in the outflow region where river-ine nutrients induced strong phytoplankton growth, resulting in high chl *a* and reduced pCO_2 in the surface layer (Tseng et al., 2011). In addition, the CO_2 distribution/uptake dynamics were yearly associated with the changes of the plume expansion determined by the CRD:

$$pCO_2 = -4.1 \times \mathrm{CRD} + 527.6, \quad R^2 = 0.96; \tag{1}$$

$$CO_2\ \text{flux} = -0.21 \times \mathrm{CRD} + 7.9, \quad R^2 = 0.97, n = 8. \tag{2}$$

where CRD is in units of $10^3\ m^3\ s^{-1}$. The results further demonstrate Changjiang river discharge governs coastal ocean production and CO_2 uptake capacity in the East China Sea shelf in summer.

3.3 Empirical algorithm to simulate seasonal pCO_{2w} variations

To derive representative mean values of pCO_{2w} in different seasons in the entire ECS shelf, we may use the strong correlation between river discharge and CO_2 uptake mentioned above (e.g., Tseng et al., 2011). We thus developed an empirical algorithm by using the monthly areal mean (referred to as "average" hereafter) of observed pCO_{2w}, and SST and the CRD during warm periods. The data mentioned above were collected during warm cruises from May to November between 1998 and 2011. Firstly, we found normalized pCO_2 at 25 °C ($NpCO_2$) correlated negatively with the CRD ($\times 10^3\ m^3\ s^{-1}$)

BGD
10, 13977–14007, 2013

with a good regression relationship (Fig. 3) as follows:

$$\mathrm{N}pCO_2 \text{ at } 25\,^{\circ}\mathrm{C} = -2.7 \times \mathrm{CRD} + 424.7 \quad (R^2 = 0.96) \tag{3}$$

Here, NpCO_2 at 25 °C, which is the observed average pCO_{2w} normalized to a constant temperature of 25 °C (mean SST of all cruises), was computed by using the following equation proposed by Takahashi et al. (1993).

$$\mathrm{N}pCO_2 \text{ at } T_{\mathrm{mean}} = (pCO_{2w})_{\mathrm{obs}} \times \exp[0.0423(T_{\mathrm{mean}} - T_{\mathrm{obs}})] \tag{4}$$

where T_{mean} is 25 °C and T_{obs} is the observed monthly mean values and $(pCO_{2w})_{\mathrm{obs}}$ is the observed average pCO_{2w}. The purpose of "pCO_2 normalized to 25 °C" is to eliminate the temperature effect in order to discern other factors (e.g., biological activities, air–sea exchange and vertical transport of subsurface waters etc.) that affect pCO_2.

The inversely linear relationship between the NpCO_2 and CRD during warm periods as shown by Eq. (1) indicates that pCO_{2w} changes in the ECS shelf water were mainly governed by biological processes, while other processes, such as the upward transport of dissolved inorganic carbon (DIC) from subsurface waters and the air–sea CO_2 exchange, are minimal under strong stratification.

We finally refined the empirical algorithm for predicting pCO_{2w} according to Eqs. (3) and (4) as below:

$$pCO_{2w} = (-2.7 \times \mathrm{CRD} + 424.7) \times e^{[0.0423 \times (T_{\mathrm{obs}} - 25)]} \tag{5}$$

where −2.7 is the slope obtained from the plot of NpCO_2 vs. CRD; CRD is the Changjing river discharge in units of $10^3\,\mathrm{m}^3\,\mathrm{s}^{-1}$; T_{obs} is the monthly average AVHRR-SST.

However, when we applied the same relationship to the cold season, we found that the relationship underestimated the NpCO_2 (Fig. 3). The extra increment was probably mainly caused by the increase in DIC provided by enhanced vertical mixing in the cold season. It is necessary to compensate for the mixing effect in the equation. As

BGD
10, 13977–14007, 2013

shown in Fig. 3, an increase of 57.4 µatm was needed to reach the observed NpCO_2 of 455.1 µatm for January from the computed NpCO_2 of 397.7 µatm, which was calculated from the CRD of 10 211 $m^3 s^{-1}$. This increment represents a 14.4 % increase to account for the mixing replenishment. For the model calculation, the seasonal mixing contribution could be estimated from the data of wind speed (W) and remotely sensed SST (T) through the relationship between the mixing ratio and the mixing index defined as W/T (see Figs. S1–S3 in Supplement materials). An enhancement factor of ca. 14.4 % could be, for instance, applied to account for the strongly vertical mixing in the months of January, February and March, when the SST was the lowest and wind speed highest during northeast monsoon. About 11.8, 8.9 and 2.4 % of the mixing ratios due to gentle mixing were for December, April and November, respectively, when the SST was higher and wind speed lower.

3.4 Time-series of model results vs. field observations

The 14 yr time-series of model results of monthly mean pCO_{2w}, δpCO_2 and the air–sea CO_2 flux in Regions S and B over the study period (1998–2011) are shown in Fig. 4, in which mean observed values of the 13 cruises are also plotted for comparison. It is clear that all modeled pCO_{2w}, δpCO_2 and the CO_2 flux agree well with the observations (Figs. 4 and S4). As shown, the time-series (Fig. 4b) is characterized by a distinct seasonal pattern with a maximum in late summer-early fall and a minimum in spring. In general, the pCO_{2w} mostly remained below pCO_{2a} throughout an annual cycle except during the period from late summer to early fall. That means the evasion of CO_2 occurred primarily in a relatively short period in the warm season. Moreover, the amount of CO_2 released was small relative to the drawndown of CO_2 in other seasons. The δpCO_2, which represents a driving potential for CO_2 gas transfer across water–air interface, seasonally fluctuated with a slight supersaturation of about +10 µatm, signifying a source of CO_2, from the ECS to atmosphere, on average in late summer and a strong undersaturation of −80 µatm, signifying a sink of atmospheric CO_2, in spring (Fig. 4c).

BGD
10, 13977–14007, 2013

There were also apparent inter-annual variations, which showed unusually high peak values in 2001, 2006 and 2011 (drought years) and exceptionally low values in 1998 and 2010 (flood years). There were anomalously strong supersaturation observed in late summer of 2001, 2006 and 2011and undersaturation in summer in 1998 and late spring in 2010, respectively, due to the Changjiang discharge fluctuations caused by climate change (Tseng et al., 2011). Subtle long-term increasing trends in pCO_{2a} and pCO_{2w} were distinctly observed:

$$pCO_{2a} = 1.9(\pm 0.0) \times t + 353.4(\pm 0.2), \quad r^2 = 0.99, n = 13 \tag{6}$$

$$pCO_{2w} = 2.1(\pm 0.8) \times t + 309.5(\pm 6.8), \quad r^2 = 0.36, n = 13 \tag{7}$$

where t = year – 1997. The pCO_{2a} has been increasing from 355.5 to 380.7 µatm at a rate of 1.9 µatm yr^{-1}, or 5.3 yr^{-1}, which is comparable to those observed at the Mauna Loa Observatory (~5.1 yr^{-1}) during the study period. The pCO_{2a} seasonality shows a spring high and a summer low. Please note the atmospheric pCO_2 observed from the cruise correlated well with the time-series data measured at JeJu Island (field pCO_{2a}(LORECS) = 1.01 × pCO_{2a}(Jeju), R^2 = 0.90, n = 13, Fig. 4b). The rate of increase in pCO_{2w} about 2.1 µatm yr^{-1} was slightly higher than that in pCO_{2a} during the study period so that δpCO_2 results showed an increase at a rate of 0.2 µatm yr^{-1}. Furthermore, if this trend was true and it continues, the uptake in the ECS will gradually decrease.

The surface pCO_{2w} and δpCO_2 (summarized in Table 1) varied seasonally and inter-annully in the ECS shelf. The annual pattern in δpCO_2 shows that negative δpCO_2 occurs in the whole year. Overall, the ECS shelf serves as a net sink of atmospheric CO_2 with −43 ± 12 µatm of δpCO_2 on average, with a strong sink in winter (−47 ± 9 µatm) and spring (−77 ± 7 µatm), and a weak sink in summer (−30 ± 32 µatm) and fall (−17 ± 17 µatm). Data from a few other cruises (spring, fall and winter) will also be used to show the complete seasonal CO_2 distribution in this region (Fig. 4c, Table 2). The average annual δpCO_2 was calculated about −48 ± 40 µatm with the seasonal variability ca. −109 µatm, −24 ± 39 µatm (n = 3), −15 µatm, and −46 µatm for

BGD
10, 13977–14007, 2013

spring, summer, fall, and winter, which were consistent with those estimated by model. The seasonal pattern shows a sink-to-source transition in late summer-early fall during the Changjiang river plume reduction after the July maximum discharge (see Fig. 6; Tseng et al., 2011). Besides, the weak sink status during warm periods is fairly sensitive to changes of pCO_2 and to become a CO_2 source due to the Changjiang discharge decreases through environmental changes (Tseng et al., 2011).

3.5 Comparison with previous estimates

Figure 5 further shows the comparison of δpCO_2 in the same month of certain year between the data retrieved from published references and this study and those generated by model. For a comparison on an equal basis, the reported fluxes had been re-calculated using the consistent source of monthly wind speed data from PenGaYi station in the ECS and the Wanninkhof's gas transfer algorithm (1992, short-term formula). In addition, the Changjiang discharges in reported references were plotted in the discharge range of climatological monthly mean with ±1 standard deviation (SD, 1998–2010) as a reference level to check anomalous events (Fig. 6a). The results show there were two flood surveys obtained in July 1992 and 2010 and others mostly lied within ±1 SD range of climatological mean. As a whole, most of published pCO_2 values are erratic away from 1 : 1 reference line outlier levels of ± 20 µatm (e.g., Peng et al., 1999; Wang et al., 2000; Shim et al., 2007; Zhai et al., 2009) while some close to model outputs (e.g., Tsunogai et al., 1999; Wang et al., 2000 in summer; Chou et al., 2011; this study). The estimates with large uncertainties are mainly due to inadequate representativeness of the spatial variability and limited sampling resolution. These problems in each report are briefly summarized in the remarks in Table 2 and the following text.

Tsunogai and coworkers (1997, 1999), for instance, reported the air–sea exchange fluxes of CO_2 in whole ECS were only extrapolated from a single transect data of the PN line across the northern ECS (Fig. 1a, Table 2). So, the findings in summer and winter applied to the whole ECS from one survey line certainly cause biases and slight higher values than the model ones (Fig. 6b and c). Their developed algorithm was

BGD
10, 13977–14007, 2013

not suitable for the use of the near-shore waters. Likewise, Peng et al's pCO_2 data (1999) were all generated from the TA and TCO_2 which were only collected in spring and limited in low-resolution samplings. Moreover, the study area of Peng et al. (1999) was mostly located in the Kuroshio, Mixed Shelf and Taiwan Warm Current waters and lacked coverage of coastal plume waters. Higher results in spring than those by model were therefore found (Fig. 6b and c), since coastal plume processes which drew the CO_2 low via phytoplankton bloom near Changjiang river mouth were not observed.

Wang et al. (2000) had only two field observations in spring and summer, while their fall and winter data were computed from the Tsunogai's empirical algorithm. Their observations lacked data from the coastal waters, although they had a wide-area survey (Fig. 1a). Hence, the spring pCO_2 data in the whole ECS, being derived from temperature–dependent relationship, were higher than those by model, which could not reflect the biological uptake by plankton bloom in the Changjiang plume (Fig. 6b and c). The summer results derived from salinity relationship were lower than the modeled ones. That was because of lack of the data from additional replenishment of CO_2 from sub-surface waters by coastal upwelling. Additionally, the fall and winter data derived from Tsunogai's algorithm could not reflect the additional CO_2 by vertical mixing during the cold seasons. Therefore, those data generated from the Tsunogai's algorithm were lower than our data by model and field observation (Fig. 6b and c).

The study in Zhai et al. (2009) was focused the areas near the Changjiang estuary so that the pCO_2 data had large fluctuations due to complexities of coastal processes with plume dynamics (Fig. 5). Low summer data were, for example, observed due to a strong bio-uptake of CO_2 relative to ones for the whole ECS while high pCO_2 in fall was due to a strong vertical mixing (Fig. 6b and c). The data of Shim et al. (2007) which were collected in the northeastern ECS showed lower in summer and higher in spring, fall and winter than model ones (Fig. 6b and c). That might be attributed to more dispersion of the Changjiang plume to the northeast of the ECS in summer at that period that drew down and the more intensive vertical mixing induced by the colder SST in cold seasons to bring the more enriched-CO_2 subsurface water to the surface, respectively.

BGD
10, 13977–14007, 2013

The comparison results further indicate small-scale spatial surveys which performed in the Changjiang estuary and northern ECS area could not be representative for the whole ECS shelf.

Chou and colleagues (2009, 2011) covered the more extensive areas like our study area so that the areal mean fluxes were rather consistent with ours. After all, the outputs from our algorithm were validated by our field observations of in-situ underway pCO_2 with high spatial and temporal resolutions since 2003 (Fig. 4b–d). The model pCO_{2w} results agreed well with the observed pCO_{2w} ($R^2 = 0.90, n = 13$; Fig. 4b). In addition, our algorithm can reflect the results caused by anomalous flood events, e.g., the floods of July in 1998 and 2010 causing exceptionally low pCO_{2w} values and high CO_2 uptakes (Table 1, Fig. 6a–c). Therefore, this assessment of annual CO_2 uptake is more credible than all previous estimates (1–3 mol C m^{-2} yr^{-1}) since our better spatial and temporal coverage reduces uncertainties.

3.6 Comparison with flux estimates by different gas-exchange algorithms

Factors that affect air–sea CO_2 flux estimates using the two-layer gas exchange model are mainly from two parts: (1) environmental forcing factors that control the gas transfer velocity, k ($m\,s^{-1}$), and (2) thermodynamic driving potentials that affect air–sea pCO_2 concentration differences (Wanninkhof et al., 2009). Among these, the parameterizations for k as a function of wind speed are largely empirical with inherent sources of uncertainty and therefore have a critical effect on the reliability of the flux estimates. Different relationships of gas exchange with wind were empirically developed by the different approaches to calculate the gas-transfer velocity over the past decades (e.g., Liss and Merlivat, 1986 (hereafter LM86); Wanninkhof, 1992 (W92: W92S, short-term; W92L, long-term); Wanninkhof and McGillis, 1999 (WM99: WM99S; WM99L); Jacobs et al., 1999 (J99); Nightingale et al., 2000 (N00); McGillis et al., 2004 (M04); Ho et al., 2006 (H06); Wanninkhof et al., 2009 (W09)). The plot of different algorithms for k against wind speed, as shown in Fig. 7, reveals that the differences among the al-

BGD
10, 13977–14007, 2013

gorithms significantly increase with wind speed increasing i.e., at low wind speeds are much less than those at high wind speeds ($> 10\,m\,s^{-1}$). In this study, the monthly average wind speed obtained from PenGaYi station in the ECS ranged between 5 and $11\,m\,s^{-1}$ with stronger winds in cold seasons during the northeast monsoon (Fig. 7). Varying up to almost three folds of differences among different algorithms for the calculation, the wind-induced k was calculated to be the highest by J99 and lowest by LM86. It further demonstrates the largest source of uncertainties involved in estimating air–sea CO_2 flux resides with these algorithms. Particularly, the differences would increase drastically among the models developed by J99, W92L and WM99L when the wind speed increases, while the algorithm developed by N00, M04 and H06 would not substantially differ, as compared to W92S (Fig. 7).

In Table 3, the summary of the averaged seasonal and annual CO_2 fluxes between 1998 and 2010 is shown for comparison, calculated from the abovementioned 10 algorithms by using monthly wind speed data measured at PenGaYi station. Overall, the averaged annual CO_2 fluxes range between -1.4 ± 0.3 and $-3.6 \pm 0.9\,mol\,C\,m^{-2}\,yr^{-1}$ with an average of -1.9 ± 0.5 (excluding the highest value by J99). The flux results can be basically divided into three groups: (i) high values (Avg: $-3.0 \pm 0.6\,mol\,C\,m^{-2}\,yr^{-1}$) by J99, W92L, and WM99L; (ii) mid-range values (-1.8 ± 0.2) by W92S, N00, M04 and H06; and (iii) low values (-1.4 ± 0.1) by LM86, WM99S and W09 (Fig. 8, Table 3). The results by W92L and WM99L are higher ca. 100 % than those by low values obtained from LM86, WM99S and W09. Among moderate values, differences in flux, compared to W92S, was not much for the algorithms developed by N00, M04 and H06 (20 % lower). The W92S was further chosen for comparison since it was widely used among the reported algorithms.

The seasonal CO_2 air–sea exchange fluxes estimated by the reported algorithms are summarized in Table 3, which highlights the differences in seasonal variability in the CO_2 sink in the ECS shelf among them. Annual CO_2 fluxes from seasonal field cruises in the ECS were also calculated by the W92S (Fig. 4d, Table 2). This is the first field dataset to show the complete seasonal CO_2 flux in this region. The average

BGD
10, 13977–14007, 2013

annual flux was calculated to be −1.9 (±1.4, seasonal variability) mol C m^{-2} yr^{-1} with the seasonal flux ca. −3.3, −0.8 ± 1.3 (n = 3), −0.6, and −3.0 mol C m^{-2} yr^{-1} for spring, summer, fall, and winter, which were almost the same as those estimated by model as shown in Table 3.

4 Conclusions

In this study, we have established an empirical relationship for predicting surface water pCO_2 in a river-dominated marginal ECS. The empirical algorithm for calculating pCO_{2w} as a function of SST and CRD successfully simulated the annual cycles of pCO_{2w}, δpCO_2 and the CO_2 flux, which are in excellent agreement with observations. The relation was further applied to the ECS shelf areas (25–33.5° N and 122–129° E) by using remotely sensed data of SST and the estimated area of CRD. Overall, the annually averaged CO_2 uptake in 1998–2011 by the ECS shelf was constrained to about 1.9 mol C m^{-2} yr^{-1}, based on observational data and model results, which were more representative than those reported previously. This assessment of annual CO_2 uptake surpasses all previous estimates in terms of temporal and spatial coverage, and, therefore, is more reliable. Thus, the ECS was annually a net sink of atmospheric CO_2 with a distinct seasonal pattern associated with inter-annual variations. The flux seasonality shows a strong sink in spring (ie., March–May) and a weak source in late summer-early fall. The weak sink status during warm periods in summer–fall is fairly sensitive to changes of pCO_2 and may be easily to shift from a sink to a source altered by shrinkage of the plume area due to the CRD decreases through environmental changes under climate change and anthropogenic forcing. The impact of Changjiang runoff change on the ECS shelf CO_2 uptake capacity shall be, therefore, highlighted in near future.

BGD
10, 13977–14007, 2013

Supplementary material related to this article is available online at: http://www.biogeosciences-discuss.net/10/13977/2013/bgd-10-13977-2013-supplement.pdf.

Acknowledgements. We thank captains and crews of R/V *OR-I* for their assistance during LORECS cruises and G.C. Gong, project PI, for cruise logistic and hydrographic data supports. Y.-F. Yeung, Y.-L. Chen, C.-S. Ji and Z.-Y. Luo assisted in lab work. This work was supported by the National Science Council (NSC, Taiwan) through grants, NSC 100 (101)-2611-M-002-004 (-015) and from the College of Science, National Taiwan University under the "Drunken Moon Lake Scientific Integrated Scientific Research Platform" grant, NTU#102R3252.

References

Cai, W. J., Dai, M. H., and Wang, Y. C.: Air-sea exchange of carbon dioxide in ocean margins: a province-based synthesis, Geophys. Res. Lett., 33, L12603, doi:10.1029/2006GL026219, 2006.

Chen, C. T. A. and Borges, A. V.: Reconciling opposing views on carbon cycling in the coastal ocean: continental shelves as sinks and near-shore ecosystems as sources of atmospheric CO_2, Deep-Sea Res. Pt. II, 56, 578–590, 2009.

Chou, W. C., Gong, G. C., Sheu, D. D., Hung, C. C., and Tseng, T. F.: Surface distributions of carbon chemistry parameters in the East China Sea in summer 2007, J. Geophys. Res., 114, C07026, doi:10.1029/2008JC005128, 2009.

Chou, W. C., Gong, G. C., Tseng, C. M., Sheu, D. D., Hung, C. C., Chang, L. P., and Wang, L. W.: The carbonate system in the East China Sea in winter, Mar. Chem., 123, 44–55, 2011.

Gong, G. C., Lee Chen, Y. L., and Liu, K. K.: Chemical hydrography and chlorophyll *a* distribution in the East China Sea in summer: implications in nutrient dynamics, Cont. Shelf Res., 16, 1561–1590, 1996.

Ho, D. T., Law, C. S., Smith, M. J., Schlosser, P., Harvey, M., and Hill, P.: Measurements of air–sea gas exchange at high wind speeds in the Southern Ocean: implications for global parameterizations, Geophys. Res. Lett., 33, L16611, doi:10.1029/2006GL026817, 2006.

BGD
10, 13977–14007, 2013

Jacobs, C. M. J., Kohsiek, W., and Oost, W. A.: Air–sea fluxes and transfer velocity of CO_2 over the North Sea: results from ASGAMAGE, Tellus B, 51(3), 629–641, 1999.

Laruelle, G. G., Dürr, H. H., Slomp, C. P., and Borges, A. V.: Evaluation of sinks and sources of CO_2 in the global coastal ocean using a spatially-explicit typology of estuaries and continental shelves, Geophys. Res. Lett., 37, L15607, doi:10.1029/2010GL043691, 2010.

Liu, K. K., Peng, T. H., and Shaw, P. T.: Circulation and biological processes in the East China Sea and the vicinity of Taiwan: an overview and a brief synthesis, Deep-Sea Res. Pt. II, 50, 1055–1064, 2003.

Liu, K.-K., Gong, G.-C., Wu, C.-R., and Lee, H.-J.: 3.2. The Kuroshio and the East China Sea, in: Carbon and Nutrient Fluxes in Continental Margins: a Global Synthesis, edited by: Liu, K.-K., Atkinson, L., Quiñones, R., and Talaue-McManus, L., IGBP Book Series, Springer, Berlin, 124–146, 2010.

Liss, P. S. and Merlivat, L.: Air-sea gas exchange rates: Introduction and synthesis, The Role of Air-Sea Exchange in Geochemical Cycling, 113–127, 1986.

McGillis, W. R., Edson, J. B., Zappa, C. J., Ware, J. D., McKenna, S. P., Terray, E. A., Hare, J. E., Fairall, C. W., Drennan, W., Donelan, M., DeGrandpre, M. D., Wanninkhof, R., and Feely, R. A.: Air-sea CO_2 exchange in the equatorial Pacific, J. Geophys. Res. 109, C08S02, doi:10.1029/2003JC002256, 2004.

Nightingale, P. D., Malin, G., Law, C. S., Watson, A. J., Liss, P. S., Liddicoat, M. I., Boutin, J., and Upstill-Goddard, R. C.: In situ evaluation of air–sea gas exchange parameterizations using novel conservative and volatile tracers, Global Biogeochem. Cy., 14, 373–387, 2000.

Peng, T. H., Hung, J. J., Wanninkhof, R., and Millero, F. J.: Carbon budget in the East China Sea in spring, Tellus B, 51, 531–540, 1999.

Shim, J., Kim, D., Kang, Y. C., Lee, J. H., Jang, S.-T., and Kim, C.-H.: Seasonal variations in pCO_2 and its controlling factors in surface seawater of the northern East China Sea, Cont. Shelf Res., 27, 2623–2636, 2007.

Takahashi, T., Olafsson, J., Goddard, J. G., Chipman, D. W., and Sutherland, S.: Seasonal variation of CO_2 and nutrients in the high-latitude surface oceans: a comparative study, Global Biogeochem. Cy., 7, 843–878, 1993.

Tseng, C. M., Wong, G. T. F., Lin, I. I., Wu, C. L., and Liu, K. K.: A unique pattern in phytoplankton biomass in low-latitude waters in the South China Sea, Geophys. Res. Lett., 32, L08608,doi:10.1029/2004GL022111, 2005.

BGD
10, 13977–14007, 2013

Tseng, C. M., Wong, G. T. F., Chou, W. C., Lee, B. S., Sheu, D. D., and Liu, K. K.: Temporal Variations in the carbonate system in the upper layer at the SEATS station, Deep-Sea Res. Pt. II, 54, 1448–1468, 2007.

Tseng, C. M., Liu, K. K., Wang, L. W., and Gong, G. C.: Anomalous hydrographic and biological conditions in the northern South China Sea during the 1997–1998 El Niño and comparisons with the equatorial Pacific, Deep-Sea Res. Pt. I, 56, 2129–2143, doi:10.1016/j.dsr.2009.09.004, 2009a.

Tseng, C. M., Gong, G. C., Wang, L. W., Liu, K. K., and Yang, Y.: Anomalous biogeochemical conditions in the northern South China Sea during the El-Niño events between 1997 and 2003, Geophys. Res. Lett., 36, L14611,doi:10.1029/2009GL038252, 2009b.

Tseng, C. M., Liu, K. K., Gong, G. C., Shen, P. Y., and Cai, W. J.: CO_2 uptake in the East China Sea relying on Changjiang runoff is prone to change, Geophys. Res. Lett., 38, doi:10.1029/2011GL049774, L24609, 2011.

Tsunogai, S., Watanabe, S., Nakamura, J., Ono, T., and Sato, T.: A preliminary study of carbon system in the East China Sea, J. Oceanogr., 53, 9–17, 1997.

Tsunogai, S., Watanabe, S., and Sato, T.: Is there a continental shelf pump for the absorption of atmospheric CO_2?, Tellus B, 51, 701–712, 1999.

Wang, S. L., Chen, C. T. A., Hong, G. H., and Chung, C. S.: Carbon dioxide and related parameters in the East China Sea, Cont. Shelf Res., 20, 525–544, 2000.

Wanninkhof, R.: Relationship between wind speed and gas exchange over the ocean, J. Geophys. Res., 97, 7373–7382, 1992.

Wanninkhof, R. and McGillis, W. R.: A cubic relationship between air–sea CO_2 exchange and wind speed, Geophys. Res. Lett., 26, 1889–1892, 1999.

Wanninkhof, R., Asher, W. E., Ho, D. T., Sweeney, C., and McGillis, W. R.: Advances in quantifying air–sea gas exchange and environmental forcing, Annu. Rev. Mar. Sci., 1, 213–244, doi:10.1146/annurev.marine.010908.163742, 2009.

Walsh, J. J.: Importance of continental margins in the marine biological cycling of carbon and nitrogen, Nature, 350, 53–55, 1991.

Weiss, R. F.: Carbon dioxide in water and seawater: the solubility of a non-ideal gas, Mar. Chem., 2, 203– 215, 1974.

Zhai, W. and Dai, M.: On the seasonal variation of air–sea CO_2 fluxes in the outer Changjiang (Yangtze River) estuary, East China Sea, Mar. Chem., 117, 2–10, 2009.

BGD
10, 13977–14007, 2013

Table 1. The seasonal and annual average CO_2 results between 1998 and 2010 in the ECS shelf.

Year		1998	1999	2000	2001	2002	2003	2004	2005	2006	2007	2008	2009	2010	**Average**
pCO_{2w} (μatm)	Spring	292 ± 12	296 ± 19	295 ± 16	290 ± 14	287 ± 30	289 ± 9	312 ± 15	299 ± 5	292 ± 7	312 ± 3	299 ± 14	293 ± 3	274 ± 20	**295 ± 10**
	Summer	262 ± 15	279 ± 31	338 ± 28	379 ± 45	315 ± 14	333 ± 45	355 ± 26	342 ± 34	365 ± 57	346 ± 11	357 ± 29	343 ± 20	296 ± 32	**331 ± 34**
	Fall	316 ± 24	320 ± 11	320 ± 15	345 ± 17	341 ± 26	354 ± 12	344 ± 4	341 ± 11	392 ± 24	356 ± 10	344 ± 22	372 ± 18	348 ± 17	**346 ± 21**
	Winter	333 ± 9	319 ± 17	319 ± 14	322 ± 10	314 ± 9	334 ± 12	326 ± 25	322 ± 4	337 ± 3	332 ± 18	330 ± 8	325 ± 8	319 ± 13	**326 ± 7**
	Annual	293 ± 26	307 ± 27	318 ± 24	333 ± 41	315 ± 27	325 ± 33	337 ± 21	325 ± 25	344 ± 48	338 ± 18	332 ± 29	335 ± 32	311 ± 35	**324 ± 15**
δpCO_2 (μatm)	Spring	−68 ± 12	−66 ± 19	−69 ± 17	−76 ± 14	−80 ± 30	−81 ± 8	−60 ± 4	−75 ± 5	−85 ± 6	−66 ± 4	−81 ± 14	−89 ± 4	−111 ± 19	**−77 ± 7**
	Summer	−88 ± 12	−74 ± 30	−16 ± 32	23 ± 49	−45 ± 18	−27 ± 49	−7 ± 31	−22 ± 39	−1 ± 62	−21 ± 15	−13 ± 33	−27 ± 25	−78 ± 37	**−30 ± 32**
	Fall	−36 ± 19	−34 ± 10	−35 ± 19	−11 ± 21	−17 ± 28	−7 ± 16	−17 ± 7	−24 ± 12	26 ± 29	−12 ± 12	−26 ± 25	1 ± 23	−26 ± 23	**−17 ± 17**
	Winter	−29 ± 10	−44 ± 18	−45 ± 15	−43 ± 11	−54 ± 10	−37 ± 14	−46 ± 27	−53 ± 5	−39 ± 5	−46 ± 19	−50 ± 9	−57 ± 10	−64 ± 13	**−47 ± 9**
	Annual	−62 ± 25	−51 ± 26	−41 ± 28	−28 ± 46	−47 ± 30	−40 ± 37	−30 ± 26	−44 ± 31	−27 ± 53	−35 ± 23	−43 ± 34	−42 ± 38	−68 ± 38	**−43 ± 12**

BGD
10, 13977–14007, 2013

Table 2. Summary of the CO_2 results in the ECS reported in the previous studies and obtained from this study.

References	Study seasons	Sampling times	Field		Model		Remarks
			[a] δpCO_2	[b] Flux	δpCO_2	Flux	
Tsunogai et al. (1997, 1999)	Summer	Aug 1994	15	1.0	−9	−0.6	1. Measured CO_2 parameters: dissolved inorganic carbon (DIC), Total alkalinity (TA), pCO_2.
	Winter	Feb ~ Mar 1993	−44	−2.4	−41	−2.2	
	Fall	Oct 1993	−26	−1.3	−23	−1.1	2. One single transect-PN line from 31.4° N, 123° E to 27.5° N, 128.4° E
		Nov 1995	−7	−0.4	−28	−1.5	
	Annual mean	1993 ~ 1995	**−55**	**−2.4**	**−41**	**−1.7**	
Peng et al. (1999)	Spring	May 1996	−28	−1.7	−93	−2.9	1. DIC, TA; 2. Two major mutually vertical transects from north-south and east-west with 14 stations in central ECS
Wang et al. (2000)	Spring	May 1995	[c] −33 [d] (−37)	−0.9 (−0.9)	−85	−2.3	1. DIC, TA 2. Wide-area survey in central and northern ECS with 26 ~ 49 stations
	Summer	Jul 1992	[c] −13 [e] (−37)	−0.6 (−1.7)	−47	−2.1	3. Lack of coastal and estuarine data
Shim et al. (2007)	Spring	May 2004	−47	−1.5	−64	−2.4	1. pCO_2
	Summer	Aug 2003	−23	−0.9	29	0.6	2.Parts of northern ECS (32–34° N, 124–128° E)
	Fall	Oct 2004	11	0.8	−21	0.7	
		Nov 2005	4	0.2	−33	−2.9	
Zhai et al. (2009)	Spring	Mar 2008	−38	−1.5	−71	−2.7	1. pCO_2
		Apr 2005	−10	−0.4	−70	−3.0	2. Outer Changjiang estuary in the inner shelf of the northwestern ECS (30–33° N, 122–124° E)
		Apr 2008	−79	−3.1	−97	−3.5	
		May 2005	−67	**−2.4**	−76	−2.7	
		Mean	**−48**	**−1.8**	**−79**	**−3.0**	
	Summer	Jul 2007	−74	−2.4	−12	**0.6**	
		Aug 2003	−45	−1.7	29	**0.6**	
		Mean	**−60**	**−2.1**	**9**	**0.0**	
	Fall	Sep 2006	22	1.1	51	2.6	
		Oct 2006	−45	**−2.7**	32	1.4	
		Nov 2006	4	0.2	−6	−0.6	
		Nov 2007	64	5.7	−24	−2.9	
		Mean	**11**	**1.1**	**13**	**0.2**	
	Winter	Jan 2006	−37	−2.3	−53	−3.0	
Chou et al. (2009, 2011)	Summer	Jul 2007	−26[c]	−1.2	−12	−0.6	1. DIC, TA, PH (Summer), DIC, TA, PH, pCO_2 (Winter)
	Winter	Jan 2008	−46	−3.0	−37	−2.5	2. the more complete ECS with 40 stations (25–32° N and 120–128° E)
This study (Tseng et al., 2011)	Spring	May 2009	−109	−3.4	−85	−2.6	1. pCO_2
	Summer	Jun 2003	−77	−2.2	−59	−1.7	2. the more complete ECS area (25–32° N and 120–128° E)
		Aug 2003	17	0.6	29	1.1	
		Jul 2004	−5	−0.3	−4	−0.2	
		Jun 2005	−47	−1.7	−67	−2.4	
		Jul 2007	−23	−0.7	−12	−0.4	
		Jul 2008	3	0.2	8	0.3	
		Jul 2009	−8	−0.4	−21	−1.0	
		Jul 2010	−103	−4.7	−91	−4.1	
		Jul 2011	−15	−0.6	−6	−0.2	
	Fall	Nov 2006	−15	−0.6	−6	−0.2	
	Winter	Jan 2008	−46	−3.0	−37	−2.5	

[a] Units in δpCO_2 and CO_2 flux are µatm and mol C m^{-2} yr^{-1}, respectively.
[b] Re-calculated by wind speed data at PenGaYi and Wnninkkhof's gas transfer algorithm (1992, short-term formula).
[c] Average of all stations.
[d] Averaged by values derived from pCO_2-salinity relationship.
[e] Averaged by values derived from pCO_2-SST relationship.

BGD
10, 13977–14007, 2013

Table 3. Seasonal average CO_2 fluxes between 1998 and 2010 derived from the reported gas-transfer algorithms.

Seasons	LM86[1]	W92L	W92S	WM99L	WM99S	J99	N00	M04	H06	W09	Range (average[2])
Spring	−2.5 ± 0.6	−4.2 ± 0.9	−3.3 ± 0.7	−3.9 ± 1.0	−2.0 ± 0.5	−5.8 ± 1.2	−2.8 ± 0.6	−2.9 ± 0.5	−2.7 ± 0.6	−2.3 ± 0.5	−2.0 ~ −5.8(−3.0)
Summer	−0.6 ± 0.6	−1.5 ± 1.7	−1.2 ± 1.3	−1.4 ± 1.7	−0.7 ± 0.8	−2.1 ± 2.3	−1.0 ± 1.1	−1.1 ± 1.2	−1.0 ± 1.1	−0.9 ± 1.0	−0.6 ~ −2.1 (−1.0)
Fall	−0.6 ± 0.5	−1.3 ± 1.2	−1.0 ± 0.9	−1.5 ± 1.4	−0.8 ± 0.7	−1.8 ± 1.6	−0.8 ± 0.8	−0.8 ± 0.7	−0.9 ± 0.8	−0.7 ± 0.6	−0.6 ~ −1.8 (−0.9)
Winter	−2.1 ± 0.4	−3.5 ± 0.8	−2.9 ± 1.1	−3.9 ± 1.1	−2.0 ± 0.5	−4.8 ± 1.4	−2.2 ± 0.5	−2.1 ± 0.4	−2.3 ± 0.5	−1.9 ± 0.4	−1.9 ~ −4.8 (−2.5)
Annual	−1.4 ± 0.3	−2.6 ± 0.7	−2.1 ± 0.5	−2.7 ± 0.7	−1.4 ± 0.4	−3.6 ± 0.9	−1.7 ± 0.4	−1.7 ± 0.5	−1.7 ± 0.4	−1.5 ± 0.4	−1.4 ~ −3.6 (−1.9)

[1] Abbreviations denote references with gas-transfer equations:
LM86: Liss and Merlivat (1986),
$k_{600} = 2.85 \times u - 9.65 (3.6 < u < 13.0)$
W92S: Wanninkhof (1992, short-term),
$k_{660} = 0.31 \times u^2$
W92L: Wanninkhof (1992, long-term),
$k_{660} = 0.39 \times u^2$
WM99S: Wanninkhof and McGillis (1999, short-term),
$k_{660} = 1.09 \times u - 0.333 \times u^2 + 0.078 \times u^3$
WM99L: Wanninkhof and McGillis (1999, long-term),
$k_{660} = 0.0283 \times u^3$
J99: Jacobs et al. (1999),
$k_{660} = 0.54 \times u^2$
N00: Nightingale et al. (2000),
$k_{600} = 0.333 \times u + 0.222 \times u^2$
M04: McGillis et al. (2004),
$k_{660} = 0.014 \times u^3 + 8.2$
H06: Ho et al. (2006),
$k_{600} = 0.266 \times u^2$
W09: Wanninkhof et al.(2009),
$k_{660} = 3 + 0.1 \times u - 0.064 \times u^2 + 0.011 \times u^3$.
[2] Average values excluding the highest data by J99.

BGD
10, 13977–14007, 2013

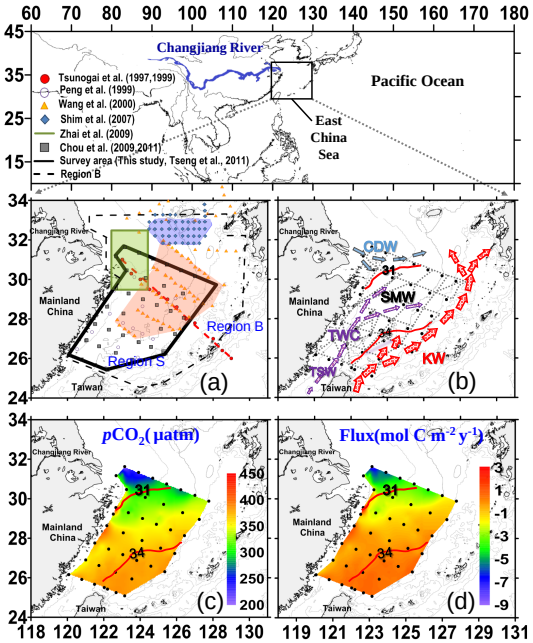

Fig. 1. Maps of the study areas in the ECS showing **(a)** the previously published CO_2-related studies (e.g., Tsunogai et al., 1997, 1999; Peng et al., 1999; Wang et al., 2000; Shim et al., 2007; Zhai et al., 2009; Chou et al., 2009, 2011; Tseng et al., 2011). The surveyed area of Tseng et al. (2011) and this study is Region S. The area outlined by dashed line for modeled synthesis is Region B. **(b)** Hydrographic stations (black dots) and cruise track of the underway pCO_2 measurements (dashed line) with sea surface salinity (SSS) contours and circulation patterns in the ECS in summer. KW–Kuroshio Water; TSW–Taiwan Strait Water; TWC–Taiwan Warm Current, SMW–Shelf Mixed Water; CDW–Changjing Diluted Water.; **(c)** the composite distributions of surface water pCO_2 (μatm); and **(d)** air–sea CO_2 exchange flux observed between August 2003 and July 2011 aboard R/V *Ocean Research-1* (OR1).

BGD
10, 13977–14007, 2013

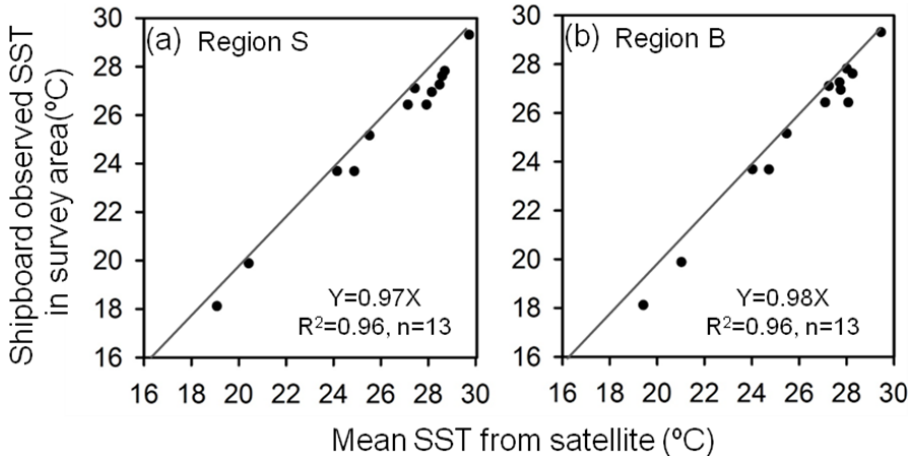

Fig. 2. Linear regression relationships between areal mean AVHRR-SST in two model regions, i.e., **(a)** S and **(b)** B, and field observed areal mean SST in cruise survey area.

BGD
10, 13977–14007, 2013

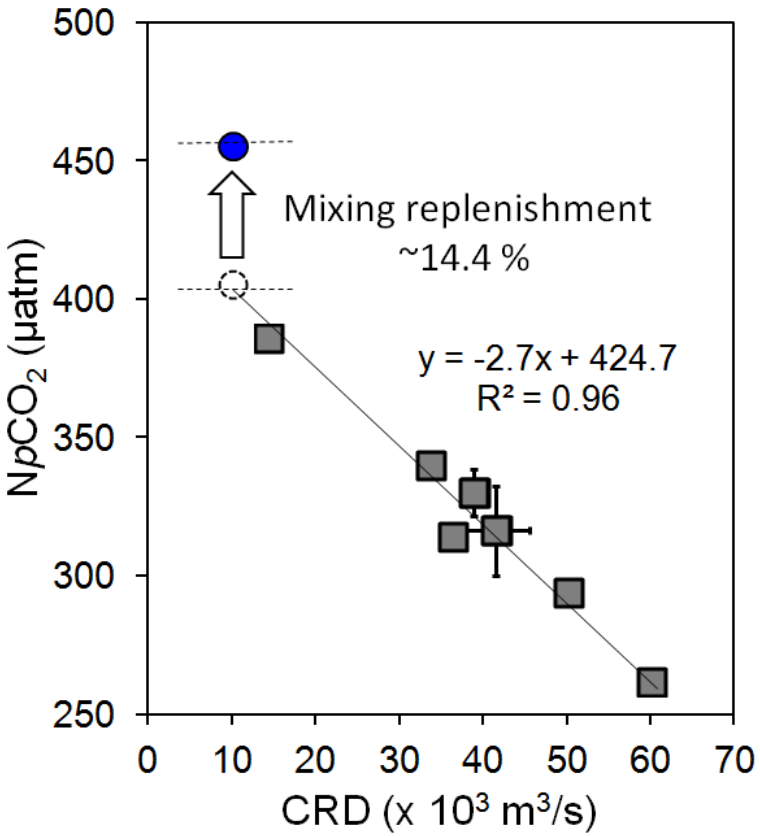

Fig. 3. Correlation between monthly average NpCO_2 and CRD (black square) was observed during warm cruises from May to November between 1998 and 2011: observed NpCO_2 about 455.1 µatm (blue dot) and the computed NpCO_2 397.7 µatm (dotted circle) at the CRD at 10 211 $m^3 s^{-1}$ during the January cruise.

BGD
10, 13977–14007, 2013

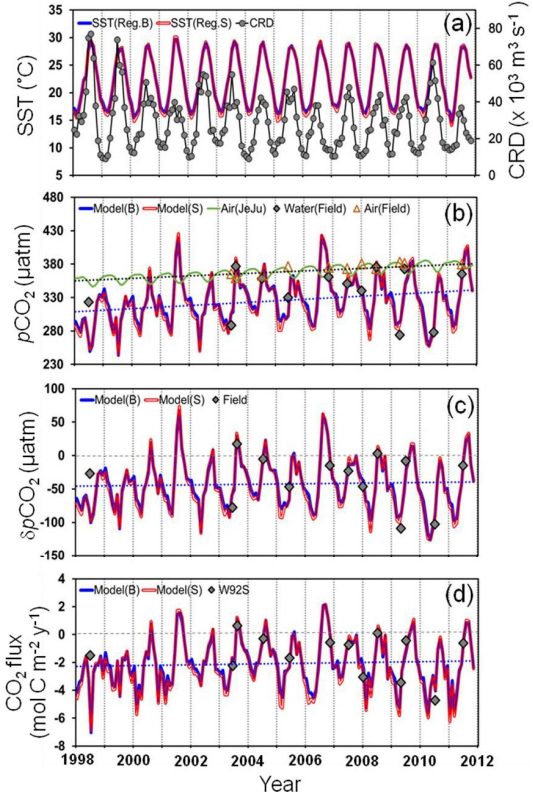

Fig. 4. Time-series variations (model results with observed data of 12 cruises) in monthly areal mean **(a)** SST and CRD, **(b)** pCO_{2w} and pCO_{2a}, **(c)** δpCO_2, and **(d)** CO_2flux in sea surface of the ECS shelf ("+": sea to air; "−": air to sea) between 1998 and 2011. The tick on the time axis corresponds to 1 January of the year marked.

BGD
10, 13977–14007, 2013

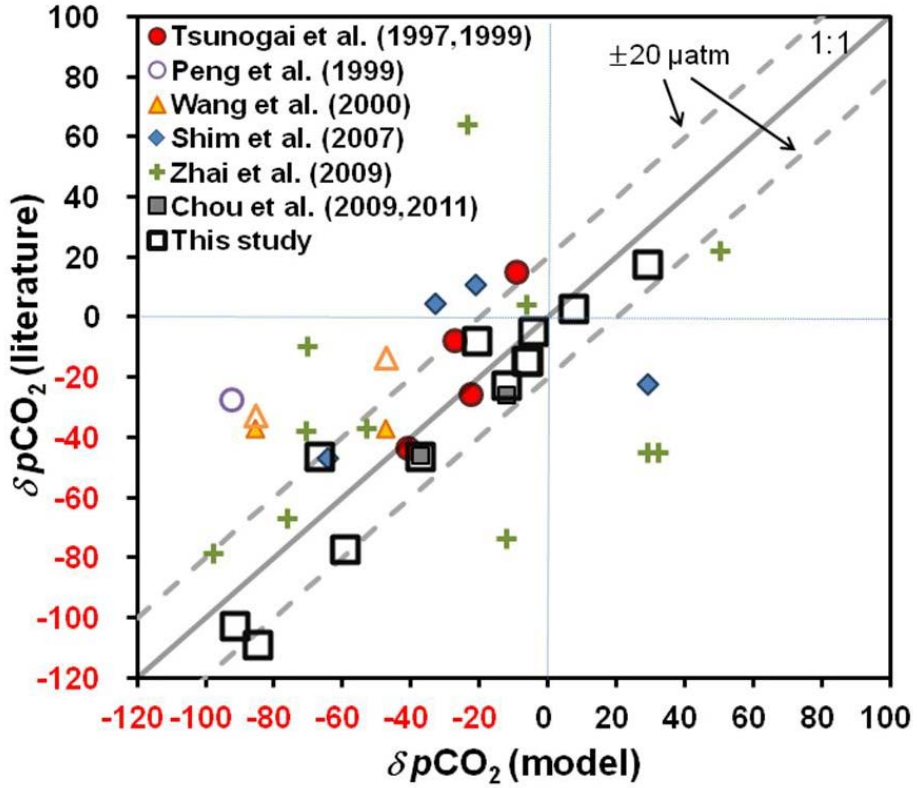

Fig. 5. δpCO_2 comparison between the data retrieved from published references and this study and those generated by model at the same surveying time.

BGD
10, 13977–14007, 2013

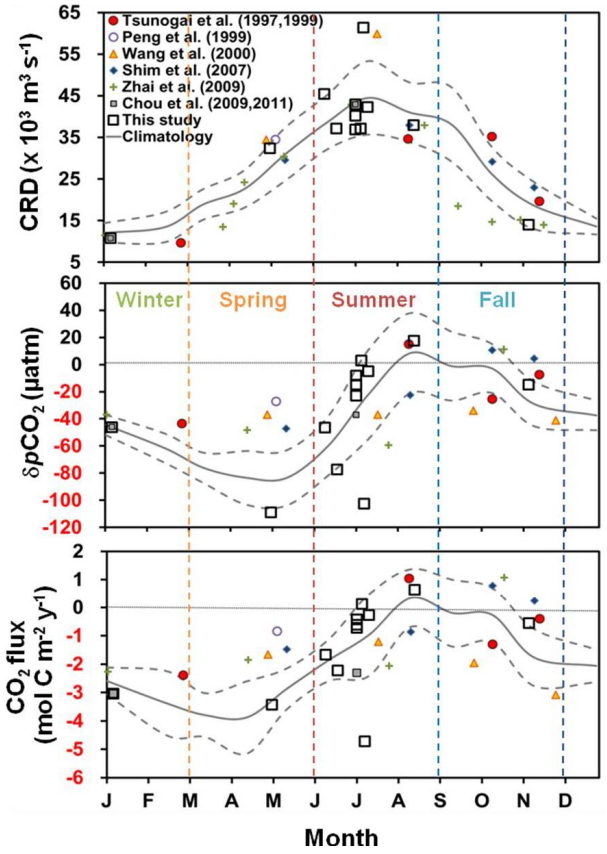

Fig. 6. Seasonal monthly patterns revealed in observational data of **(a)** CRD, **(b)** $\delta pCO_2$and **(c)** air–sea CO_2 flux, obtained from published references and from field data in this study and model results. The thick curves denotes the climatological mean and the dash curves denote the range of ±1 SD during the study period of 1998–2011.

BGD
10, 13977–14007, 2013

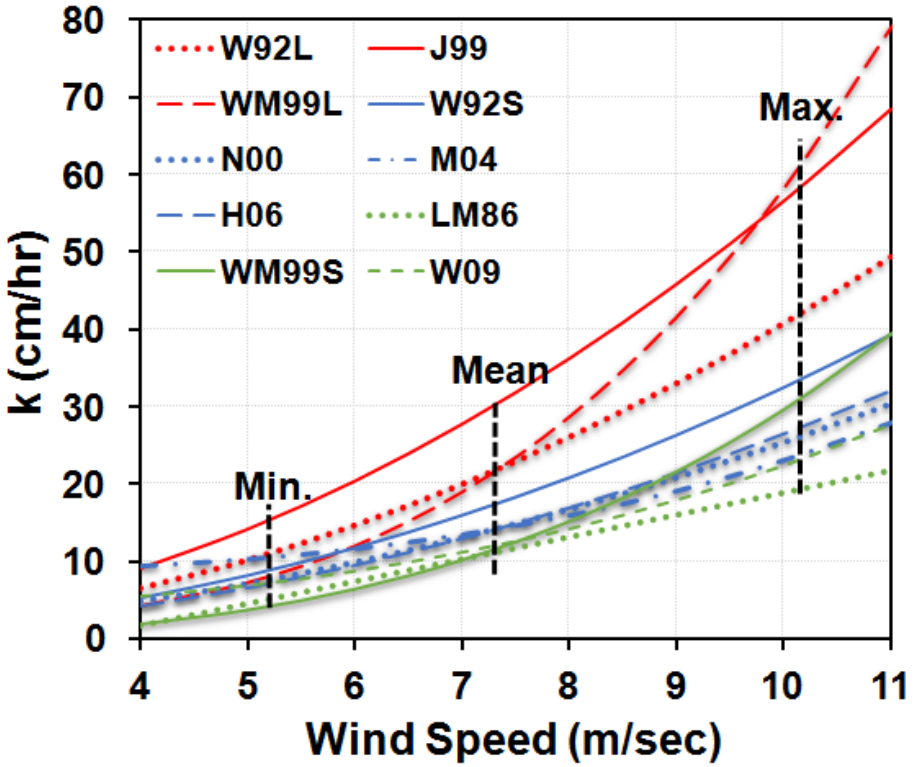

Fig. 7. Comparison among different algorithms for flux calculation against wind speed (LM86 corresponds to Liss and Merlivat (1986); other labels see in Table 3). Black dashed lines in Min., Mean and Max. denote the minimum, average and maximum monthly average wind speeds obtained from PenGaYi station in the ECS during the study period.

BGD
10, 13977–14007, 2013

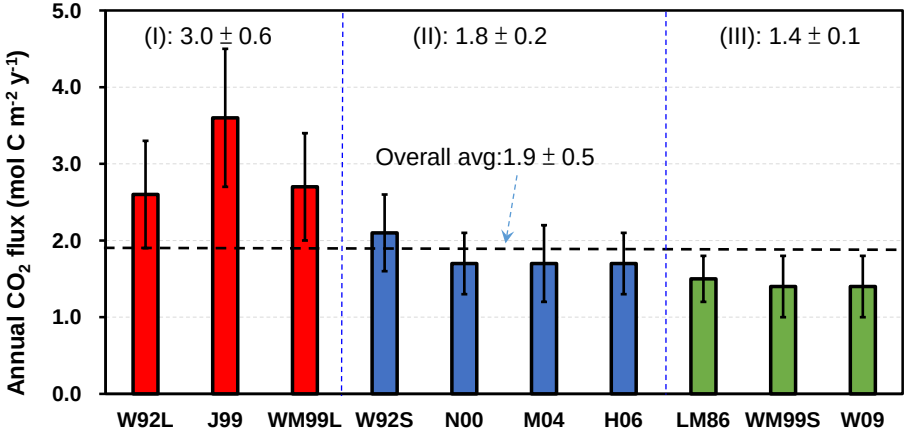

Fig. 8. Comparison among the averaged annual CO_2 fluxes estimated by different algorithms in the study period. Three distinctive groups: (i) highest average: $-3.0 \pm 0.6\,\mathrm{mol\,C\,m^{-2}\,yr^{-1}}$; (ii) mid-range: -1.8 ± 0.2; (iii) low values: -1.4 ± 0.1 with an overall average: -1.9 ± 0.5.

BGD
10, 13977–14007, 2013